OPEN ACCESS Freely available online

AFM Applied Functional Materials

ISSN 2737-5323
Volume 3, Issue 2
https://www.iikii.com.sg/journal/AFM
Applied Functional Materials

Article Type (Article)

Effect of Ga Concentration on the Output Performance of ZnO Piezoelectric Nanorods Nanogenerator

Tung-Lung Wu [1], Teen-Hang Meen [2,*] , and Yu-Chuan Chang [2]

[1] School of Mechanical and Automotive Engineering, Zhaoqing University, Zhaoqing, Guangdong 516260, China
[2] Department of Electronic Engineering, National Formosa University, Huwei Township, Yunlin County 632, Taiwan
* Correspondence: thmeen@gs.nfu.edu.tw

Received: Apr 30, 2023**; Revised:** May 15, 2023**; Accepted:** Jun 1, 2023**; Published:** Jun 30, 2023

Abstract: In this study, a self-assembled monolayer of octyltriethoxysilane was grown on ITO glass. Subsequently, a hydrothermal method was employed to grow low-density gallium (Ga)-doped zinc oxide (ZnO) nanorod structures. In this growth process, the undoped pure ZnO nanorods and ZnO nanorods doped with five different Ga concentrations were developed. After growing the nanorods, X-ray diffraction (XRD) analysis was conducted on both undoped pure ZnO and Ga-doped ZnO nanorods to observe the influence of Ga concentration on the crystalline structure of the ZnO nanorods. Additionally, scanning electron microscopy (SEM) was utilized to examine changes in the surface and cross-sectional growth of ZnO nanorods with varying Ga concentrations, thereby investigating the impact of Ga concentration on the growth of ZnO nanorods. Finally, a thin Pt film was sputtered onto the ZnO nanorod structures to assemble nanogenerators. Ultrasonic excitation was applied to develop these nanogenerators for electrical measurements, allowing us to explore the effects of metal doping on the nanorods' electrical properties.

Keywords: Ga-doped ZnO nanorods, ITO substrate, piezoelectric properties, nanogenerator

1. Introduction

Electricity has long been an indispensable component of human daily life. Traditional methods of electricity generation rely on the combustion of coal, oil, and natural gas as fuel sources, but the associated greenhouse gas emissions and the finite nature of these resources have posed persistent concerns. In recent years, the impacts of global warming and energy crises have become increasingly pronounced, underscoring the need for more sustainable energy solutions. Self-powering systems represent a groundbreaking approach eliminating the need for external power sources or batteries. These systems autonomously harvest and utilize energy from their surrounding environment to meet the electricity demands of various products and devices. Common examples of self-powering systems encompass solar self-powering systems [1], vibration energy harvesting systems [2], thermal energy harvesting systems [3], and RF energy harvesting systems [4]. The applications of self-powering systems are exceptionally diverse, encompassing a wide range of fields such as IoT devices, wearable technology, and wireless sensors, among others. This innovative technology not only offers a source of clean and sustainable energy but also fosters self-sufficiency by reducing dependence on conventional batteries. Moreover, it provides extended and dependable power capabilities, contributing to a more resilient and environmentally friendly future.

Emerging zinc oxide (ZnO) materials have exhibited one-dimensional (1-D) nanostructural characteristics, with different fabrication methods yielding various nanostructures. Over the past decade, the synthesis of ZnO nanostructures, such as nanorods, nanobelts, and nanoparticles, has been continuously successful. Among these structures, nanorods are the most representative. Nanotechnology leverages these nanomaterials to assemble structures with specific properties by utilizing their unique characteristics. Nanostructures such as quantum dots and quantum wells, for instance, can be applied to light emission or light sensing. Conversely, when light interacts with these nanostructures, it changes its inherent properties due to their interactions with one another. This advancement in ZnO nanostructures and nanotechnology holds promise for a wide range of applications, from photonics to electronics, offering opportunities to tailor and enhance the performance of various devices and systems.

ZnO one-dimensional nanostructures not only serve as a fundamental basis for research in various material properties such as optical, electrical, magnetic, and mechanical characteristics but also hold tremendous potential in nanophotonics and nanoelectronics due to their unique optoelectronic properties. They are applied to a wide range of nanophotonic devices, including light-emitting diodes (LEDs), field emission devices, surface coatings for conductive materials, laser diodes (LDs), solar cells [5], gas sensors,

photonic crystals, field-effect transistors (FETs), and photodetectors [6]. Furthermore, ZnO is classified as a piezoelectric semiconductor material. When fabricated in thin-film form, it can be utilized in surface acoustic wave devices (SAW devices). In its one-dimensional form, it can be applied in nanogenerator devices, which harness mechanical energy at the nanoscale to generate electrical power. These diverse applications demonstrate the versatility and promise of ZnO nanostructures in advancing various technologies across multiple domains [7].

In publications, the fabrication of ZnO nanorods can be broadly categorized into two primary methodologies: gas-phase and liquid-phase methods. Gas-phase techniques encompass methodologies such as Metal Organic Chemical Vapor Deposition (MOCVD), Pulse Laser Deposition (PLD), and high-temperature furnace chemical vapor deposition. In contrast, liquid-phase methods include Electrophoresis, Template-based approaches, and the Hydrothermal method. In this particular study, we adopted the Hydrothermal method, a liquid-phase technique, for the growth of ZnO nanorods [8,9]. This method offers several compelling advantages, including low-temperature synthesis, cost-effectiveness, ease of fabrication, and the production of materials with reduced defects and a higher rate of success compared to alternative approaches. The Hydrothermal method's versatility and favorable attributes make it a preferred choice for the production of high-quality ZnO nanorods.

In nanotechnology, a wide array of applications, including nanoscale gas sensors, health-monitoring nano-biosensors, biological detectors, nanorobots, and wearable devices, grapple with a common challenge: the depletion of batteries and the ensuing need for replacements. This predicament not only demands significant time and effort but also contributes to the problem of waste generation, in line with the principles of sustainability. Moreover, many of these applications demand uninterrupted, round-the-clock operation to fulfill their intended functions. A promising solution to this predicament lies in the integration of nanogenerators with self-powering systems. Nanogenerators are used for various energy sources in tandem with self-sustaining power systems with the potential to supplant conventional batteries as the primary power source. This shift not only ensures sustainable and continuous operation but also eliminates the need for frequent battery replacements, thereby reducing both cost and environmental impact. This combination of nanogenerators and self-powering systems represents a significant step toward greener, more efficient, and more reliable nanotechnology applications.

Self-powering nanogenerators, which serve as an innovative source of energy for various applications, operate by ingeniously converting environmental mechanical energy sources such as sound waves, vibrations, and fluid motion into usable electrical power [10,11]. This approach offers several compelling advantages. First and foremost, the energy sources harnessed by nanogenerators are readily available in the surrounding environment, making them essentially inexhaustible. This stands in stark contrast to traditional batteries that require periodic replacement or recharging which is cumbersome and costly. Moreover, the ability of nanogenerators to autonomously harvest energy from their environment enables components and devices to operate continuously without interruption. This uninterrupted functionality is crucial for many applications, especially in healthcare, environmental monitoring, and remote sensing, where reliability is paramount. Furthermore, nanoscale devices typically demand relatively modest power levels to function efficiently. This not only extends the operational lifespan of the nanogenerator but also eliminates the constraints imposed by traditional battery capacity and size. As a result, products incorporating nanogenerators become more lightweight and portable, offering enhanced convenience and usability [13]. In essence, the integration of self-powering nanogenerators represents a significant advancement in energy harvesting technology, offering sustainable and uninterrupted power sources and revolutionizing a wide range of applications, from wearable technology to environmental monitoring systems.

In this study, we initially deposited a self-assembled monolayer of octadecyltrimethoxysilane on an ITO glass substrate. Subsequently, we employed a hydrothermal method to grow low-density gallium (Ga)-doped ZnO nanorod structures on the substrate. After growing these nanorod structures, we sputter-coated a thin Pt film onto the nanostructures. This assembly of components constitutes a nanogenerator. We then utilized ultrasonic waves to drive the nanogenerator and conducted electrical measurements to investigate the impact of metal doping on the nanorod structures. This research was conducted to understand how the introduction of metals, specifically Ga in this case, influences the electrical properties and performance of the nanorod structures within the nanogenerator.

2. Materials and Methods

The nanogenerator was constructed on an ITO (indium tin oxide) glass substrate, serving as the foundation for the growth of ZnO nanorods. The fabrication process began with meticulous substrate preparation, involving a sequence of cleaning steps using acetone, isopropanol, and deionized water. After thorough cleaning, the substrate was carefully dried in an oven. Next, a thermal deposition was initiated by placing the substrate within a Teflon container and introducing 0.2 mL of octadecyltrichlorosilane. This container was then sealed and subjected to a high-pressure autoclave environment, where was heated to 150°C for 60 min. This controlled thermal treatment resulted in the creation of a self-assembled monolayer on the substrate surface, enhancing its properties for subsequent processes. The hydrothermal growth of ZnO nanorods was the subsequent stage of the fabrication process, and it

was achieved through the utilization of zinc nitrate ($Zn(NO_3)_2$), hexamethylenetetramine ($C_6H_{12}N_4$), and gallium nitrate ($Ga(NO_3)_3$) as the precursor materials, and their used ratios are shown in Table 1. In this study, the effects of different precursor ratios were investigated by observing their surface and cross-sectional morphologies by SEM. This growth process was performed at a controlled temperature of 95°C for a period of 12 h. After the completion of nanowire growth, the substrate surface was meticulously rinsed with deionized water to eliminate any remaining impurities, ensuring the integrity of the nanogenerator.

To enhance the voltage and current output of the nanogenerator and ultimately boost its power generation capacity, a platinum layer was deposited onto the surface of ZnO nanorods by using the sputtering method to serve as the conductive layer. Subsequently, two substrates with overlapping nanowire arrays were encapsulated using a protective polymeric film, completing the fabrication of the nanogenerator. The schematic diagram of the nanogenerator is presented in Figure 1 and the physical diagram of the fabricated nanogenerator component is shown in Figure 2. The final step involved material analysis and electrical measurements. In this research, an innovative approach was proposed to enhance the performance of the nanogenerator. Ga was introduced through a process of metal doping into the ZnO nanorods. The study comprised a series of analyses, including surface morphology analysis, X-ray spectroscopy dispersion analysis, X-ray diffraction analysis, and electrical analysis. These analyses aimed to investigate the influence of metal doping on the performance and characteristics of the nanogenerator.

Table 1. Pharmaceutical parameters of Ga-doped ZnO nanorods grown by low-temperature hydrothermal method.

Materials	Ratio
$Zn(NO_3)_2$:HMTA	25 mM:25 mM
$Zn(NO_3)_2$:HMTA:$Ga(NO_3)_3$	25 mM:25mM:1 mM
$Zn(NO_3)_2$:HMTA:$Ga(NO_3)_3$	25 mM:25 mM:1.5 mM
$Zn(NO_3)_2$:HMTA:$Ga(NO_3)_3$	25 mM:25 mM:2 mM
$Zn(NO_3)_2$:HMTA:$Ga(NO_3)_3$	25 mM:25 mM:2.5 mM
$Zn(NO_3)_2$:HMTA:$Ga(NO_3)_3$	25 mM:25 mM:5 mM

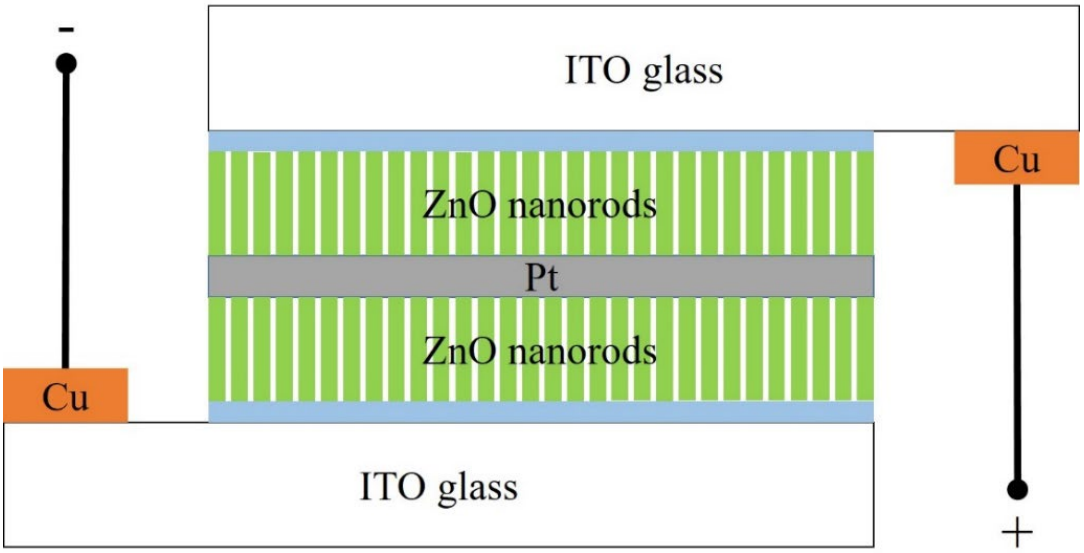

Figure 1. Schematic diagram of nanogenerator.

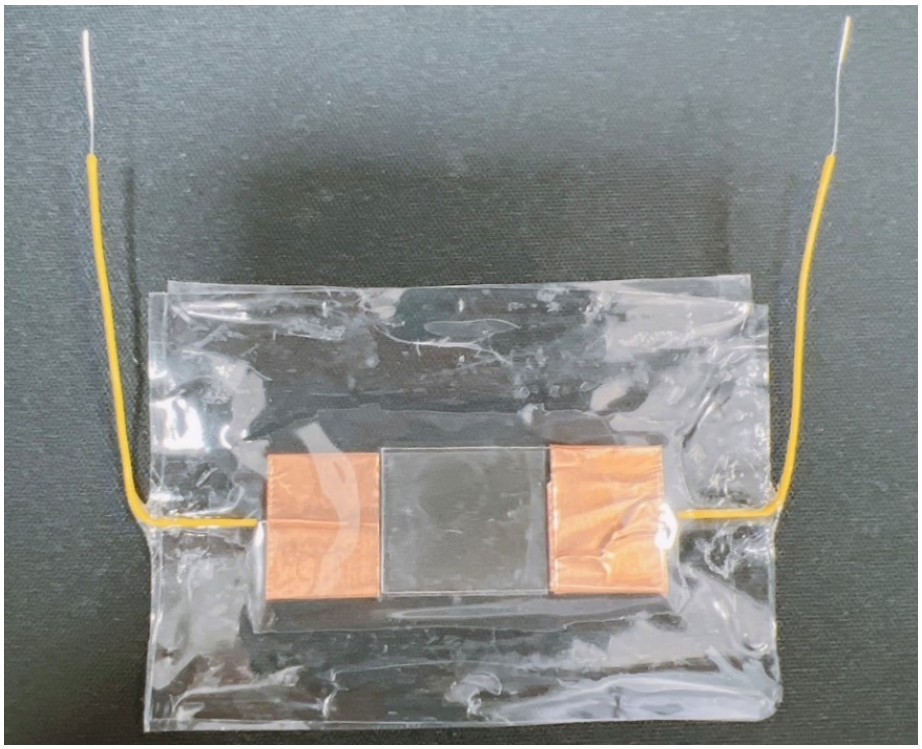

Figure 2. Physical diagram of nanogenerator components.

3. Results and Discussions

The primary materials used in this experiment were zinc nitrate and hexamethylenetetramine, serving as the main sources for the growth of ZnO nanorods. Zinc nitrate dissociates into zinc ions in water, while hexamethylenetetramine hydrolyzes to produce ammonia. Subsequently, ammonia reacts with the hydroxide ions generated in the water and zinc ions to form ZnO. The reaction is illustrated as follows [45].

$$Zn(OH)_2 \leftrightarrows ZnO + H_2O \quad (1)$$

$$Zn^{2+} + 2OH^- \leftrightarrows Zn(OH)_2 \quad (2)$$

$$NH_3 \bullet H_2O \leftrightarrows NH_4^+ + OH^- \quad (3)$$

$$NH_3 + H_2O \leftrightarrows NH_3 \bullet H_2O \quad (4)$$

$$(CH_2)_6N_4 + 6H_2O \leftrightarrows 4NH_3 + 6HCHO \quad (5)$$

The concentration of hydroxide ions is a crucial factor in the growth of ZnO, making hexamethylenetetramine a pivotal player in providing these hydroxide ions. Hexamethylenetetramine exhibits a slow and uniform hydrolysis rate, which allows for the gradual release of hydroxide ions. This results in a low and stable concentration of hydroxide ions in the solution, maintaining a pH level of approximately 6 to 7. Additionally, within the reaction, hexamethylenetetramine forms complexes with zinc ions, adsorbing around the growing ZnO nanocrystals. This mobility of complexes aids in the unidirectional growth of one-dimensional ZnO nanorods. The aforementioned reaction induces self-assembled molecular films to capture ZnO and form ZnO nanorods. In an aqueous solution, to facilitate the chain reaction with compounds in the water and generate materials that form ZnO nanostructures with appropriate energy input, it is crucial to properly tailor the overall reaction for nanorod formation. When the reaction solution is in a low-concentration state, it accelerates the precipitation of ZnO, causing the substrate to fail to efficiently capture ions in the aqueous solution, resulting in poorer growth conditions. Conversely, in a high-concentration state, the reaction solution allows the substrate to capture ions from the aqueous solution more effectively, leading to the formation of structurally more uniform ZnO nanorods. The reaction rate is critical in the formation of ZnO nanorods. When the reaction rate is too rapid, it accelerates the precipitation of ZnO, hindering the self-assembled molecular film's ability to effectively capture ions from the aqueous solution and resulting in suboptimal growth conditions. On the other hand, when the reaction rate is too slow, it prevents the formation of ZnO compounds, ultimately impeding the formation of the desired ZnO nanorod structures.

In this experiment, the surface morphology of ZnO nanorods was analyzed using scanning electron microscopy (SEM) to observe variations in the morphology of ZnO nanorods at different doping concentrations and make comparisons. Figure 3(a) presents an overhead view of pure ZnO nanorods, it can be observed that the tops of the nanorods exhibit an asymmetrical hexagonal structure with a width of approximately 0.46 μm. In Figure 3(b), the cross-sectional view of pure ZnO nanorods reveals that the nanorods primarily grow vertically upwards from the substrate, with a length of approximately 8.62 μm. Figure 3(c) displays an overhead view of Ga-doped ZnO nanorods with a 1 mM concentration. The tops of the nanorods exhibit an asymmetrical hexagonal structure with a width of approximately 1.32 μm. In Figure 3(d), the cross-sectional view of these doped nanorods indicates that the primary growth direction remains vertical upwards from the substrate, with a length of approximately 9.32 μm. Finally, in Figure 3(e), an overhead view of Ga-doped ZnO nanorods with a 1.5 mM concentration reveals that the tops of the nanorods exhibit an asymmetrical hexagonal structure with a width of approximately 1.47 μm. Figure 3(f), the corresponding cross-sectional view, demonstrates that the nanorods still predominantly grow vertically upwards from the substrate, with a length of approximately 11.2 μm.

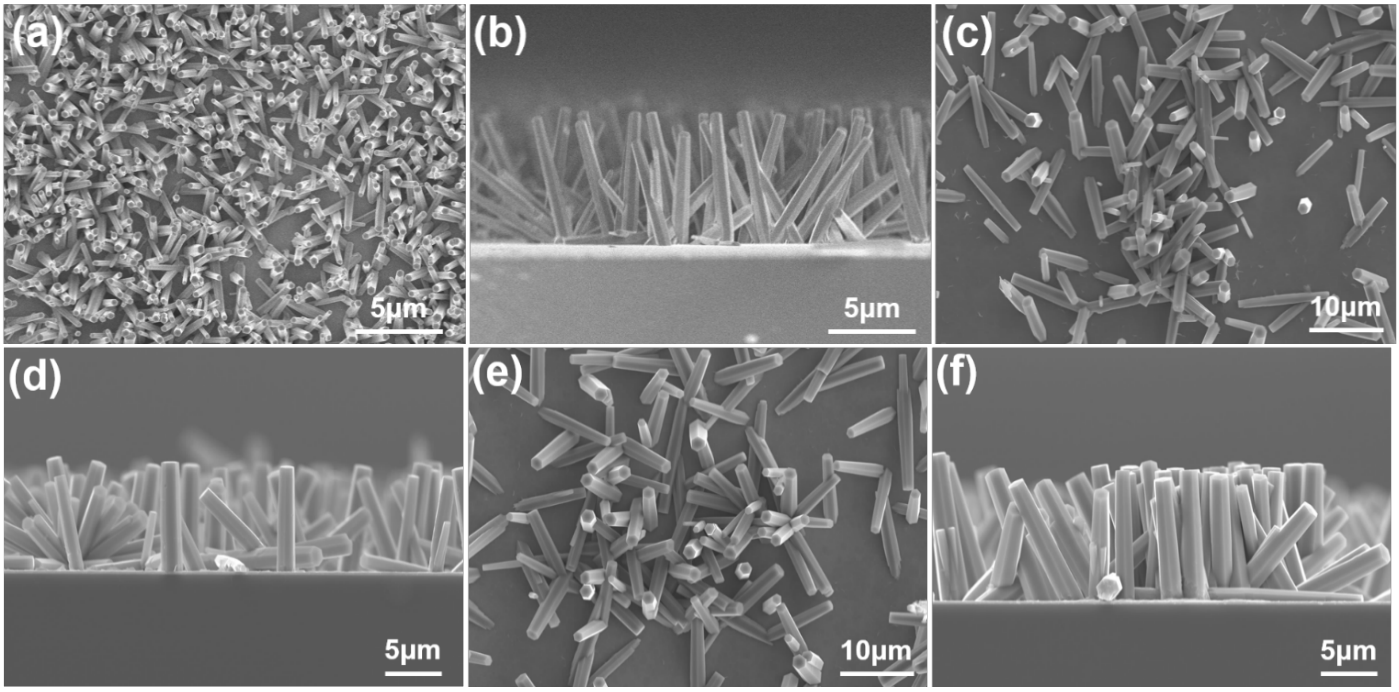

Figure 3. SEM images of (a) top view and (b) side view of pure ZnO nanorods, (c) top view and (d) side view of 1 mM Ga-doped ZnO nanorods, and (e) top view and (f) side view of 1.5 mM Ga-doped ZnO nanorods.

Figure 4(a) presents a top-down view of 2 mM Ga-doped ZnO nanorods. The top of the nanorods exhibits an asymmetrical hexagonal structure with a width of approximately 1.62 μm. In Figure 4(b), the cross-sectional view of the same 2 mM Ga-doped ZnO nanorods reveals that the primary growth direction of the nanorods is vertical, extending upward from the substrate, with a length of approximately 16.5 μm. Figure 4(c) presents a top-down view of 2.5 mM Ga-doped ZnO nanorods. Similar to the previous case, the top of these nanorods exhibits an asymmetrical hexagonal structure, with a width of around 1.74 μm. Figure 4(d) shows the cross-sectional view of these 2.5 mM Ga-doped ZnO nanorods that primarily grow vertically upward from the substrate, with a length of approximately 8.14 μm. Figure 4(e) illustrates a top-down view of 5 mM Ga-doped ZnO nanorods. These nanorods also display an asymmetrical hexagonal structure at their tops, with a width of approximately 1.22 μm. In Figure 4(f), the cross-sectional view of the 5 mM Ga-doped ZnO nanorods is presented. Their predominant growth direction is vertical, with a length of approximately 9.86 μm. Table 2 provides a comparison of the lengths and widths of the ZnO nanorods at different Ga concentrations. The top-down view shows that Ga-doped ZnO nanorods, despite having a lower density compared to pure ZnO nanorods, have a larger width. The cross-sectional view shows that the length of the nanorods increases with increasing doping concentration, but after reaching a certain concentration, both length and width start to decrease. The 2 mM Ga-doped ZnO nanorods have the longest length and exhibit the best vertical growth characteristics.

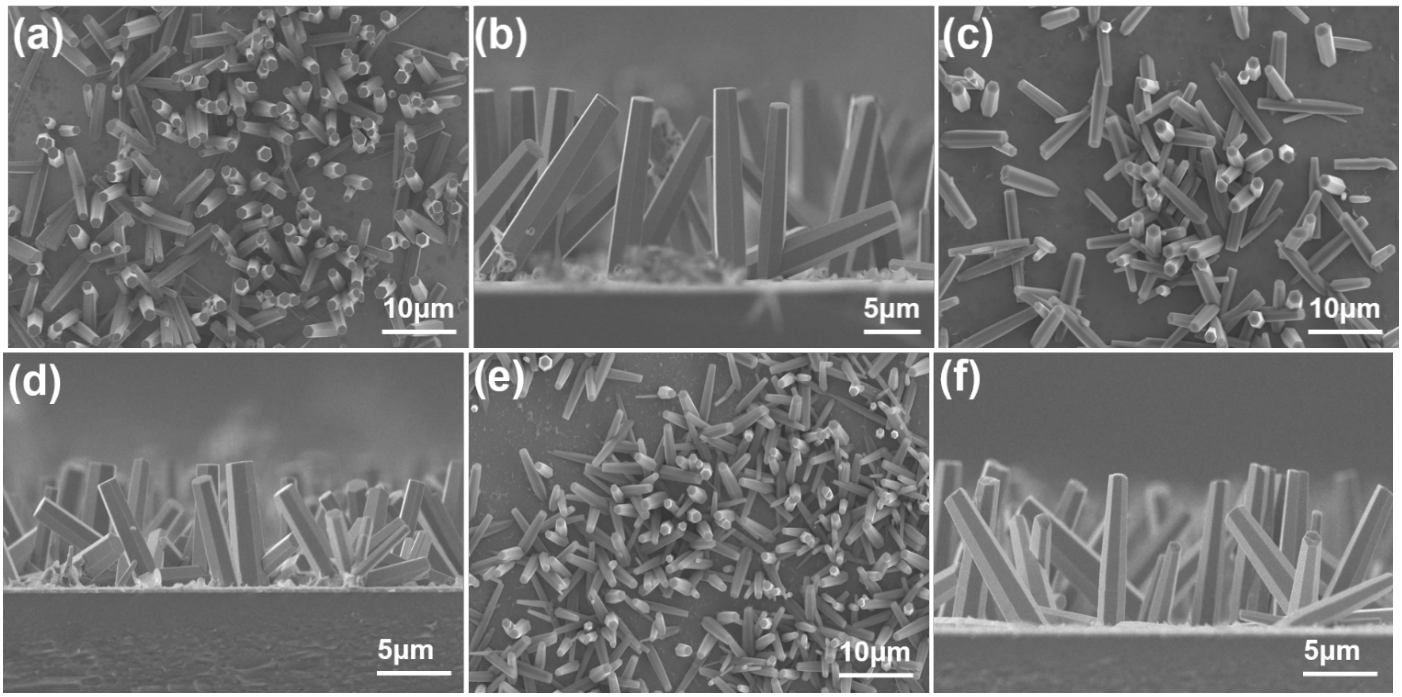

Figure 4. SEM images of (a) top view and (b) side view of 2.0 mM Ga-doped ZnO nanorods, (c) top view and (d) side view of 2.5 mM Ga-doped ZnO nanorods, and (e) top view and (f) side view of 5.0 mM Ga-doped ZnO nanorods.

Table 2. Comparison of nanorods' lengths and widths at different Ga concentrations.

Ga concentration	0 mM	1 mM	1.5 mM	2 mM	2.5 mM	5 mM
width	0.46 μm	1.32 μm	1.47 μm	1.62 μm	1.74 μm	1.22 μm
length	8.62 μm	9.32 μm	11.2 μm	16.5 μm	8.14 μm	9.86 μm

In this experiment, the main components of the nanorods and the proportion of doped elements were analyzed using an Energy Dispersive Spectroscopy (EDS) attachment on a scanning electron microscope. The analysis results for 1 and 5 mM are shown in Figures 5(a) and 5(b). In the EDS analysis charts, it is observed that the atomic percentages of Ga, doped at different concentrations, are 0.49 (1 mM), 0.62 (1.5 mM), 0.71 (2 mM), 1.20 (2.5 mM), and 1.50 (5 mM). It is evident that with an increase in doping concentration, the atomic percentage of Ga also increases, confirming the presence of Ga doping within the ZnO nanorods. Furthermore, elemental distribution maps provide additional confirmation of the existence of Ga within the ZnO nanorods. This EDS analysis not only confirms the successful incorporation of Ga into the ZnO nanorods but also quantifies the extent of doping. The increasing atomic percentages of Ga with higher doping concentrations align with expectations, indicating a successful doping process. These findings have significant implications for the properties and applications of the doped ZnO nanorods, as the concentration of the dopant element can influence their electrical, optical, and chemical characteristics. The ability to precisely control doping levels is essential for tailoring nanorod properties to specific applications in fields such as optoelectronics, sensors, and catalysts.

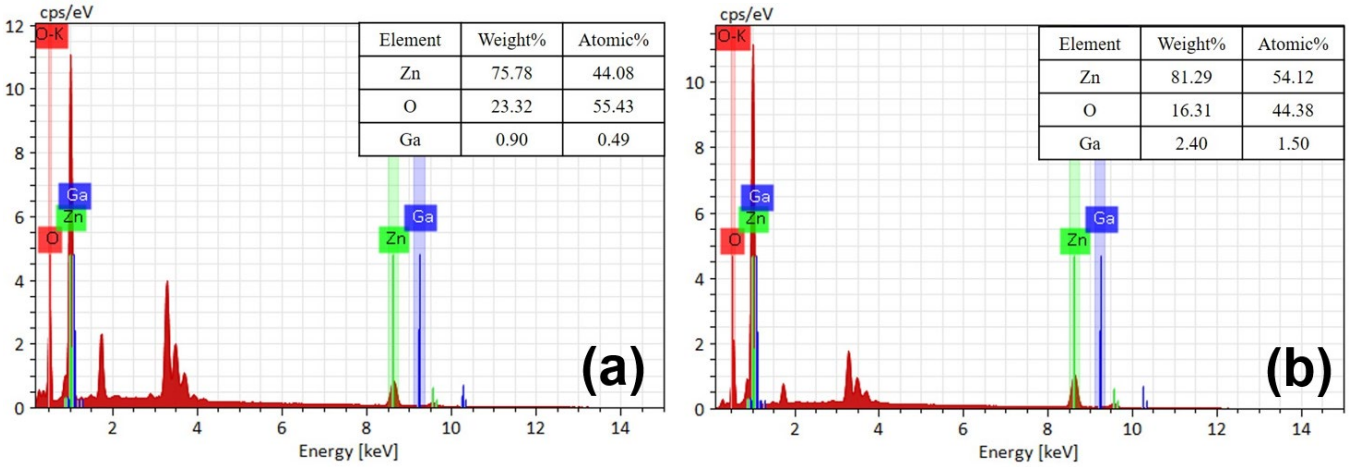

Figure 5. EDS analyses of (a) 2.0 mM Ga-doped ZnO nanorods and 5.0 mM Ga-doped ZnO nanorods.

The diagram in Figure 6 illustrates the crystal facets of Ga-doped ZnO nanorods grown via a hydrothermal method. The analysis result using JADE software confirmed a prominent peak at 34.4° corresponding to the (002) crystal facet of ZnO, indicating that the Ga-doped ZnO nanorods grow along the vertical substrate direction (C-axis direction). Additionally, minor peaks were observed at 31.7°, 36.2°, 47.4°, 56.5°, 62.7°, and 67.8°, corresponding to (100), (101), (102), (110), (103), and (112) facets of ZnO, respectively. These peaks, although representing ZnO facets, were not as pronounced, possibly due to gaps or spacing between the nanorods, leading to measurements of adjacent crystal facets. It is noteworthy that the (002) peak, associated with 2 mM Ga doping, exhibited the highest intensity, indicating the strongest crystalline structure among the samples.

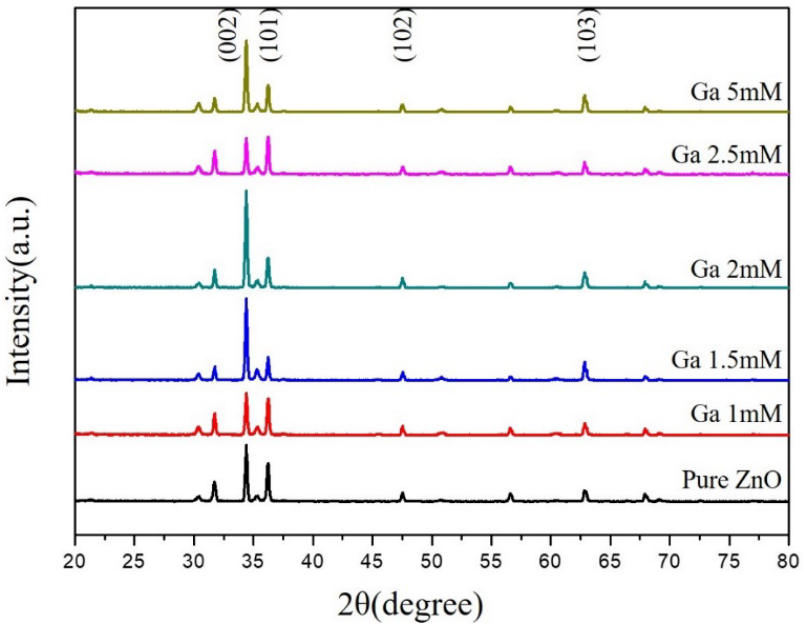

Figure 6. XRD patterns of the undoped and Ga-doped ZnO nanorodes.

We compared the power generation efficiency of nanogenerators made with pure ZnO and those doped with five different concentrations of Ga. The nanogenerator devices had a measurement area of 2 × 1.5 cm. Electrical characterization was carried out using a multifunctional source meter (Keithley 2400) and an ultrasonic cleaner operating at 42K Hz. We confirmed the presence of Schottky contact curves by measuring the IV characteristic curves of the nanogenerators. Subsequently, we measured the average current and average voltage. The ultrasonic cleaner was activated for 30 s, followed by a 30-second pause, and this cycle was repeated for a total measurement duration of 210 S. This methodology allowed us to assess the electrical performance of the nanogenerators. When the concentration of added Ga varied, the power generation characteristics of ZnO differed. Taking pure ZnO as an example, its I-V characteristic curve confirmed good Schottky contact between the metal and the oxide layer. When the voltage varied from -3 to +3 V, the corresponding current changed from -10.53 to 15.69 mA. The average current measured at zero

voltage was 2.81×10^{-8} A and the average voltage measured at zero current was 4.96×10^{-5} V. Under these conditions, the obtained average power was 1.39×10^{-12} W.

Figure 7 shows the power generation characteristics of a 2mM Ga-doped ZnO nanorods nanogenerator. The I-V characteristic curve in Figure 7(a) confirms that there is good Schottky contact between the metal and the ZnO layer, with currents ranging from -32.13 to 31.23 mA corresponding to voltages from -3 to +3 V. The average current measured at zero voltage is 3.39×10^{-7} A (Figure 7(b)), and the average voltage measured at zero current is 1.13×10^{-3} V (Figure 7(c)). The obtained average power is 3.83×10^{-10} W. Table 3 provides a comparison of various parameters. The highest average power is obtained when the Ga doping concentration is 2mM, surpassing that of pure ZnO. Furthermore, the I-V curves show that the voltage and current stability are optimal at a Ga doping concentration of 2mM. The most symmetrical Schottky curve is achieved at a Ga doping concentration of 2.5mM.

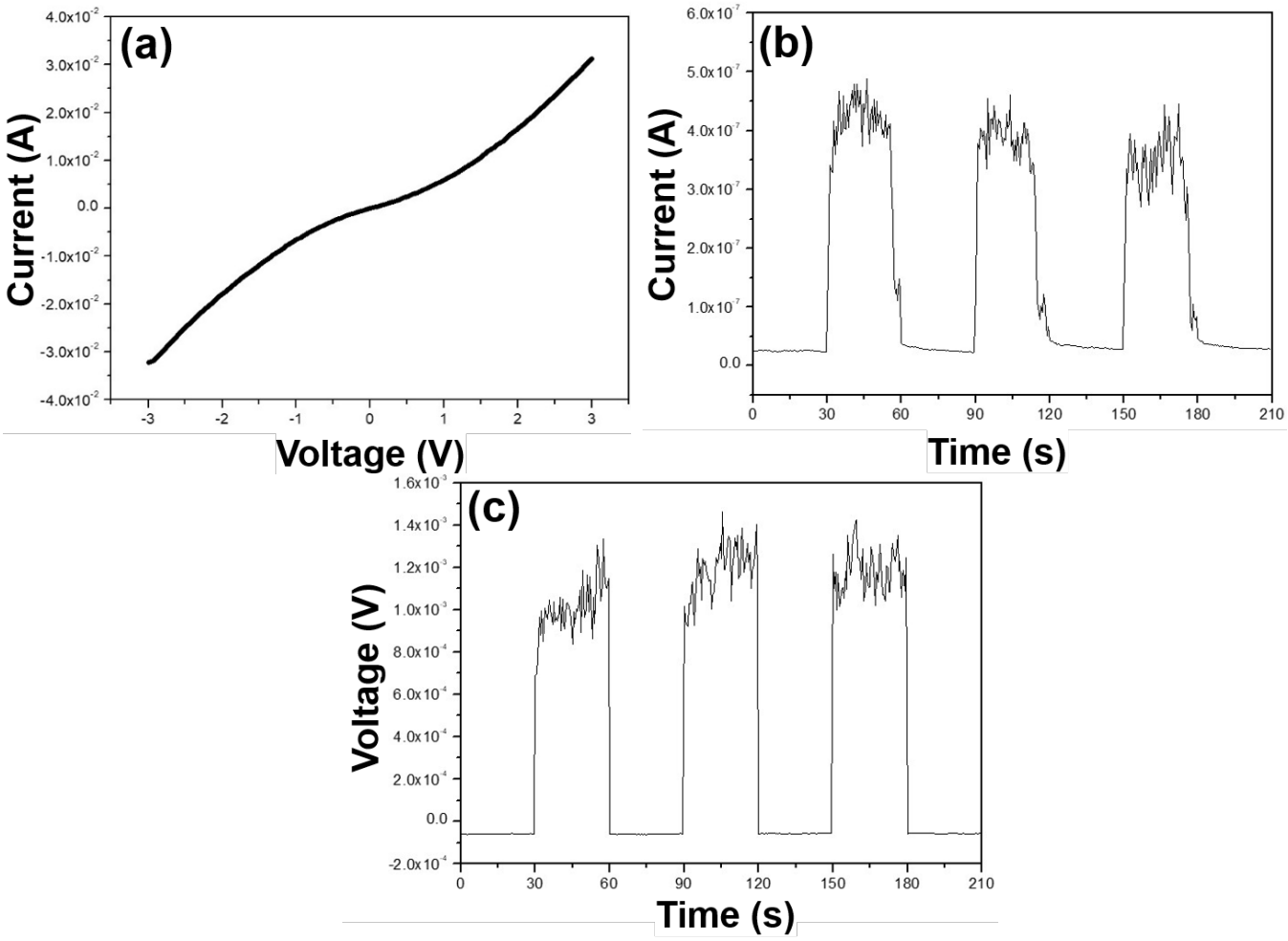

Figure 7. 2mM Ga-doped ZnO nanorods nanogenerator power generation characteristics (a) I-V curve diagram, (b) average current diagram, and (c) average voltage diagram.

Table 3. Effect of Ga concentration on the average current, average voltage, average power, and power gain of the fabricated nanogenerators.

Ga concentration	Average current (A)	Average voltage (V)	Average power (W)	Power gain factor
ZnO	2.81×10^{-8}	4.96×10^{-5}	1.39×10^{-12}	
1 mM	2.20×10^{-8}	6.71×10^{-4}	1.47×10^{-11}	10.57
1.5 mM	1.35×10^{-7}	9.92×10^{-5}	1.33×10^{-11}	9.56
2 mM	3.39×10^{-7}	1.13×10^{-3}	3.83×10^{-10}	275.53
2.5 mM	2.59×10^{-7}	5.19×10^{-4}	1.34×10^{-10}	96.40
5 mM	7.07×10^{-8}	5.62×10^{-4}	3.97×10^{-11}	28.56

4. Conclusions

The length and width of Ga-doped ZnO nanorods increase as the Ga concentration increases. However, when a certain concentration is reached, a decrease in nanorod length is observed for 2.5mM and 5mM Ga doping, with the best dimensions found for 2mM Ga-doped ZnO nanorods. The increase in Ga concentration is accompanied by an increase in the proportion of Ga in the nanorods, which was confirmed by elemental analysis from EDS. The EDS elemental distribution maps precisely depicted the distribution of Ga within the nanorods, providing further evidence of Ga incorporation. XRD analysis results revealed that Ga doping enhances the intensity of the main peak (002) compared to the pure ZnO nanorods. The introduction of Ga into the ZnO nanorods expanded the crystal lattice, leading to an internal piezoelectric effect. The increase in nanorod length enhanced the external piezoelectric effect when subjected to external vibrations, thereby improving the efficiency of the nanogenerator. Electrical characterization measurements were conducted by placing the nanogenerator in an ultrasonic bath and using a Keithley 2400 multifunction source meter. The average power output for 2mM Ga-doped ZnO nanorods was found to be 3.83×10^{10} W, indicating the highest power generation efficiency among the tested samples.

Author Contributions: Writing—original draft preparation, T. H. Meen; Formal analysis, Y. C. Chang.

Funding: This research did not receive external funding.

Conflicts of Interest: The authors declare no conflict of interest.

References

1. Song, W.; Yin, X.; Liu, D.; Ma, W.; Zhang, M.; Li, X.; Cheng, P.; Zhang, C.; Wang, J.; Wang, Z. A highly elastic self-charging power system for simultaneously harvesting solar and mechanical energy. *Nano Energy* **2019**, *65*, 103997.
2. Birgin, B.H.; García-Macías, E.; D'Alessandro, A.; Ubertini, F. Self-powered weigh-in-motion system combining vibration energy harvesting and self-sensing composite pavements. *Construction and Building Materials* **2023**, *369*, 130538.
3. Tuoi, T. T. K.; Toan, N.V.; Ono, T. Self-powered wireless sensing system driven by daily ambient temperature energy harvesting. *Applied Energy* **2022**, *311*, 118679.
4. Xie, Y.; Long, J.; Zhao, P.; Chen, J.; Luo, J.; Zhang, Z.; Li, K.; Han, Y.; Hao, X.; Qu, Z.; et al. A self-powered radio frequency (RF) transmission system based on the combination of triboelectric nanogenerator (TENG) and piezoelectric element for disaster rescue/relief. *Nano Energy* **2018**, *54*, 331–340.
5. Mwankemwa, B.S.; Malevu, T.D.; Sahini, G.M.; Vuai, A.S. Effects of vertically aligned ZnO nanorods surface morphology on the ambient-atmosphere fabricated organic solar cells. *Results in Materials* **2022**, *14*, 100271.
6. Xu, N.; Yuan, Z.; Wang, B.; Nie, F.; He, J.; Wang, X. Significant improvement in the performance of well-aligned ZnO nanowire arrays ultraviolet photodetector by Ga doping. *Microelectronic Engineering* **2022**, *260*, 11178.
7. Kaur, J.; Singh, H. Fabrication and analysis of piezoelectricity in 0D, 1D and 2D Zinc Oxide nanostructures. *Ceramics International* **2020**, *46* (11), 19401–19407.
8. Tam, K. H.; Cheung, C. K.; Leung, Y. H.; Djurišić, A. B.; Ling, C. C.; Beling, C. D.; Ding, L. Defects in ZnO nanorods prepared by a hydrothermal method. *The Journal of Physical Chemistry B* **2006**, *110*(42), 20865–20871.
9. Yang, C.; Wang, C.; Wang, F.; Liu, H; Micova, J. Growth of ZnO Nanoflower Arrays on a Patterned Sapphire Substrate. *Apply. Function. Mater*. **2022**, *2*, 44–50.
10. Rafique, S.; Kasi, A.K.; Aminullah; Kasi, J.K.; Bokhari, M.; Shakoor, Z. Fabrication of Br doped ZnO nanosheets piezoelectric nanogenerator for pressure and position sensing applications, *Current Applied Physics* **2021**, *21*, 72–79.

11. Manjula, Y.; Rakesh, K.R.; Missak Swarup Raju, P.; Anil Kumar, G.; Venkatappa Rao, T.; Akshaykranth, A.; Supraja, P. Piezoelectric flexible nanogenerator based on ZnO nanosheet networks for mechanical energy harvesting, *Chemical Physics* **2020**, *533*, 110699.